ACADEMIC PRESS

Available online at www.sciencedirect.com

SCIENCE DIRECT®

Journal of Magnetic Resonance 163 (2003) 215–227

JMR Journal of Magnetic Resonance

www.elsevier.com/locate/jmr

Implications of using approximate Bloch–McConnell equations in NMR analyses of chemically exchanging systems: application to the electron self-exchange of plastocyanin

D. Flemming Hansen and Jens J. Led*

Department of Chemistry, University of Copenhagen, Universitetsparken 5, DK-2100 Copenhagen Ø, Denmark

Received 23 December 2002; revised 21 February 2003

Abstract

The validity of a series of approximate solutions of the Bloch–McConnell equations normally applied in the analyses of chemically exchanging systems is evaluated, using the electron self-exchange (ESE) in the blue copper protein plastocyanin from *Anabaena variabilis* as an example. The evaluation is based on a comparison with the results of a complete analysis of the NMR signals of chemically exchanging nuclei that allows an independent and accurate determination of all the involved parameters. The complete analysis is based on the general solution of the Bloch–McConnell equations. It includes a simultaneous analysis of the chemical shift, and the transverse and longitudinal relaxation rates of the observed nuclei as well as the variation of these parameters with the molar fractions of the exchanging species and the rate of the chemical exchange process. The linear prediction model method was used in the data analysis to achieve the highest possible precision. Surprisingly, it is found that the fast exchange condition may not be fulfilled even in cases where a single exchange-averaged NMR signal is observed, and the Larmor frequency and relaxation rates depend linearly on the molar fractions of the exchanging species. In such cases the use of approximate solutions in the analysis of the transverse relaxation rates and the pseudo-contact shifts can lead to erroneous results. In limiting cases close to the fast exchange and slow exchange regimes correct values of some of the parameters can be obtained using the second order approximate solution of the Bloch–McConnell equations. In contrast, the complete analysis of the NMR signals results in an accurate determination of the exchange rates and the NMR parameters of the exchanging sites. This, in turn, can provide information about the structure and function of a protein undergoing chemically exchange. For the investigated plastocyanin the complete analysis results in an accurate determination of the paramagnetic enhancement of the nuclear relaxation rates, the paramagnetic chemical shift, the electron relaxation rate, the electron self-exchange rate, and the distances between the nuclei and the paramagnetic metal ion, viz. the Cu^{2+} ion.

Keywords: Chemical exchange; Electron self-exchange; Bloch–McConnell equations; Paramagnetic NMR; *Anabaena variabilis* plastocyanin

1. Introduction

In quantitative NMR studies of chemically exchanging proteins in solution an accurate analysis of the NMR signals is imperative. This holds *inter alia* for paramagnetic metallo-proteins, where valuable information about the dynamics, structure, and function of the proteins can be obtained from an accurate determination of the relaxation rates and Larmor frequencies of the protein nuclei [1–5].

In chemically exchanging systems, the nuclei reside itinerantly in different conformations that may be characterized by different NMR parameters. Depending on the size of the exchange rate and the difference between corresponding NMR parameters of the exchanging sites, a given nucleus either give rise to a single exchange-averaged signal, or to separate signals corresponding to the individual conformations. In both cases, the NMR signals may depend on more than one of the conformations and can, therefore, provide information

* Corresponding author. Fax: +45-3535-0609.
E-mail address: led@kiku.dk (J.J. Led).

1090-7807/$ - see front matter © 2003 Elsevier Science (USA). All rights reserved.
doi:10.1016/S1090-7807(03)00062-4

about all of the involved conformations as well as the exchange process.

The NMR signals of chemically exchanging systems are described by the Bloch–McConnell equations [6,7]. If a sufficiently versatile dataset is available, all the relevant NMR parameters of a chemically exchanging system can be determined simultaneously using the *general* solution of these equations. However, because of limited experimental information approximate solutions of the Bloch–McConnell equations [8] are often used to obtain information about systems of biological interest, the specific form of the equations being dependent on the system under investigation, the applied experimental conditions, and the type of data available. In the case of a limited dataset, approximate solutions of the equations may be used incorrectly and can, therefore, result in erroneous estimates of the parameters. This was clearly emphasized in a recent theoretical study of relaxation in the rotating frame of a system outside the fast exchange limit [9]. Moreover, the available dataset may be analyzed using non-optimal computational procedures.

Here we present an evaluation of the approximate solutions of the Bloch–McConnell equations of a chemically exchanging system. The evaluation is based on a comparison with the results of a complete analysis of the NMR signals of chemically exchanging nuclei that allows an independent and accurate determination of all the involved parameters. The complete analysis is based on the general solution of the Bloch–McConnell equations. It includes a simultaneous analysis of the chemical shift, and the transverse and longitudinal relaxation rates of the observed nuclei as well as the variation of these parameters with the molar fractions of the exchanging species and the rate of the chemical exchange process. The specific protein under investigation is the blue copper protein, plastocyanin from *Anabaena variabilis* (*A.v.* PCu). In partly oxidized blue copper proteins an electron self-exchange (ESE) causes the nuclei to exchange between two forms characterized by different NMR parameters, i.e., the reduced, diamagnetic form and the oxidized, paramagnetic form.

2. Experimental

2.1. Sample preparation

A sample of plastocyanin (PCu) from the blue green bacteria *Anabaena variabilis* (*A.v.*), prepared and purified as described previously [10], was supplied by Prof. Jens Ulstrup, the Technical University of Denmark. The protein was dissolved in 99.9% D_2O at pH 6.9–7.1 (meter reading). The partly oxidized samples were prepared by mixing the appropriate amounts of the reduced and the oxidized form of *A.v.* PCu. The protein concentrations of the samples used in the NMR experiments were 0.08, 0.47, 0.53, 0.95, and 1.89 mM, respectively, and the molar fraction, f_p, of oxidized *A.v.* PCu was in the range from 0.00 to 0.92. All samples contained 50 mM NaCl.

2.2. Determination of the molar fraction of the oxidized species

The fraction, f_p, of oxidized *A.v.* PCu was estimated from the longitudinal relaxation rates of nuclei that fulfill the fast exchange condition ($R_{1p} \ll k_{ese}c$), as described previously [3]. Here R_{1p} is the paramagnetic longitudinal relaxation enhancement, k_{ese} is the second order rate constant for the ESE process, and c is the total concentration of the protein. The molar fraction, f_p, of oxidized *A.v.* PCu was determined with an absolute uncertainty of 0.002–0.02 using this approach. The rates were normalized using a freshly prepared 5% oxidized sample in which the degree of oxidation was determined optically, using the strong absorbance at 597 nm of the oxidized form.

2.3. NMR experiments

Non-selective, one-dimensional inversion recovery R_1 experiments were carried out at 298.2 K and a ^1H frequency of 500 MHz, using a Varian Unity Inova 500 spectrometer. The ^1H carrier was placed on the HDO resonance located at 4.77 ppm relative to TMS at 298.2 K [11]. The number of data points in the spectra was 32768 and the sweep width was 9000 Hz in the non-selective inversion recovery R_1 experiments. Eleven relaxation delays, τ, in the range from 10 ms to 8.00 s were used in these experiments.

2.4. Data analysis using the linear prediction model method

The experimental data were analyzed using the linear prediction model method [12] as described previously [12,13]. The first step of this method is a fast linear prediction (FLP) analysis [14] of the individual FIDs corresponding to the different τ delays in the R_1 experiments. This analysis provides the number of signals in the spectra together with estimates of the four spectral parameters of each of the predicted signals, that is, the intensity, $I(\tau)$, the frequency, ν, the linewidth, $\Delta\nu_{1/2}$, and the phase, ϕ. Also the analysis gives the uncertainties of the parameters and their mutual correlations.

The number of signals found by the FLP calculations may differ from one FID to another in an inversion recovery experiment, or the spectral parameters of the predicted signals may be heavily correlated because of severe overlap. Consequently, the estimated parameters of closely spaced signals are often distributed in an

unpredictable way among the signals. Therefore, a direct fit of the model to the obtained parameters is difficult and may lead to erroneous results for closely spaced signals.

The linear prediction model method alleviates this problem by creating a set of auxiliary FIDs from the spectral parameters obtained by the FLP analysis. Thus, for each experimental FID an auxiliary FID is created corresponding to the specific spectral region of interest. This approach ensures that the information contained in the auxiliary FIDs is exactly the same as in the original experimental data that describes the spectral region. Subsequently, the particular model describing the data is fitted simultaneously to the complete set of auxiliary FIDs to obtain the relevant parameters.

3. Theory

A simple, general system, where a nucleus exchanges between two distinct magnetic environments, A and B, with different chemical shift and different relaxation rates of the nucleus, is considered, that is

$$A \underset{k_B}{\overset{k_A}{\rightleftharpoons}} B, \tag{1}$$

where k_A and k_B are the exchange rates out of site A and B, respectively.

3.1. The longitudinal magnetization

After a pertubation, and under the free-precession Hamiltonian, the macroscopic Bloch–McConnell equations describing the time dependence of the longitudinal magnetization in the presence of chemical exchange can be written as [7]

$$\dot{M}_{z,A} = R_{1,A}(M^{\infty}_{z,A} - M_{z,A}) - k_A M_{z,A} + k_B M_{z,B}, \tag{2}$$

$$\dot{M}_{z,B} = R_{1,B}(M^{\infty}_{z,B} - M_{z,B}) - k_B M_{z,B} + k_A M_{z,A}. \tag{3}$$

Here $\dot{M}_{z,j}$ is the time derivative of the longitudinal magnetization $M_{z,j}$ in site j, where $j = A, B$, while $M^{\infty}_{z,j}$ is the corresponding equilibrium longitudinal magnetization, and $R_{1,j}$ is the corresponding longitudinal relaxation rate in the absence of exchange. The general solution of Eqs. (2) and (3) takes the form [7,15,16]:

$$M_{z,A}(\tau) = \Lambda_1 e^{\lambda_1 \tau} + \Lambda_2 e^{\lambda_2 \tau} + M^{\infty}_{z,A}, \tag{4}$$

$$M_{z,B}(\tau) = \Lambda_3 e^{\lambda_1 \tau} + \Lambda_4 e^{\lambda_2 \tau} + M^{\infty}_{z,B}, \tag{5}$$

where

$$\lambda_1 = 1/2\left\{ -(k_{1A} + k_{1B}) + \sqrt{(k_{1A} - k_{1B})^2 + 4k_A k_B} \right\}, \tag{6}$$

$$\lambda_2 = 1/2\left\{ -(k_{1A} + k_{1B}) - \sqrt{(k_{1A} - k_{1B})^2 + 4k_A k_B} \right\}, \tag{7}$$

$$\Lambda_1 = \{(\lambda_2 + k_{1A})(M^{\infty}_{z,A} - M^0_{z,A}) - k_B(M^{\infty}_{z,B} - M^0_{z,B})\}/(\lambda_1 - \lambda_2), \tag{8}$$

$$\Lambda_2 = \{-(\lambda_1 + k_{1A})(M^{\infty}_{z,A} - M^0_{z,A}) + k_B(M^{\infty}_{z,B} - M^0_{z,B})\}/(\lambda_1 - \lambda_2), \tag{9}$$

$$\Lambda_3 = \{-k_A(M^{\infty}_{z,A} - M^0_{z,A}) - (\lambda_1 + k_{1A}) \times (M^{\infty}_{z,B} - M^0_{z,B})\}/(\lambda_1 - \lambda_2), \tag{10}$$

$$\Lambda_4 = \{k_A(M^{\infty}_{z,A} - M^0_{z,A}) + (\lambda_2 + k_{1A}) \times (M^{\infty}_{z,B} - M^0_{z,B})\}/(\lambda_1 - \lambda_2) \tag{11}$$

and

$$k_{1A} = R_{1,A} + k_A,$$

$$k_{1B} = R_{1,B} + k_B.$$

In Eqs. (8)–(11), $M^0_{z,j}$ denotes the initial longitudinal magnetization, $M_{z,j}(\tau)$, for $\tau = 0$. It should be noted that the time dependences of the magnetizations are in general bi-exponential. In practice, it is not possible to separate the two eigenvalues λ_1 and λ_2 from a single bi-exponential recovery [16] when $\lambda_2/\lambda_1 \leqslant 5$, [16] because of the non-orthogonal character of the two exponential functions, $e^{\lambda_1 \tau}$ and $e^{\lambda_2 \tau}$. Therefore, approximations must be made, or more informative experiments must be applied as demonstrated previously for the analysis of the longitudinal magnetization [16], and here in the form of a simultaneous analysis of the time dependences of the longitudinal and transverse magnetizations and the chemical shifts. Also, to ensure the retrieval of maximum information from the experimental data, sophisticated fitting procedures can be applied, such as the linear prediction model method used in the analysis here.

3.2. The transverse magnetization

The macroscopic Bloch–McConnell equations describing the time dependence of the transverse magnetization in the presence of chemical exchange take the form [15]:

$$\dot{M}_{xy,A} = -(R_{2,A} - i\omega_A)M_{xy,A} - k_A M_{xy,A} + k_B M_{xy,B}, \tag{12}$$

$$\dot{M}_{xy,B} = -(R_{2,B} - i\omega_B)M_{xy,B} - k_B M_{xy,B} + k_A M_{xy,A} \tag{13}$$

in the absence of the rf-field. Here $\dot{M}_{xy,j}$ is the time derivative of the transverse magnetization $M_{xy,j}$ in site j, where $j = A, B$, while $R_{2,j}$ and ω_j denote the corresponding transverse relaxation rate of the macroscopic magnetic moment, and the Larmor frequency, respectively, in the absence of exchange. Eqs. (12) and (13) are equivalent to Eqs. (2) and (3) if the following substitutions are made: $M^{\infty}_{z,j} \mapsto 0$ and $R_{1,j} \mapsto R_{2,j} - i\omega_j$. Therefore, the general solution of Eqs. (12) and (13) can be

found by substituting $M_{z,j}^{\infty} \mapsto 0$ and $R_{1,j} \mapsto R_{2,j} - i\omega_j$ in the solution of the longitudinal magnetizations, that is

$$M_{xy,A}(t) = \Theta_1 e^{\vartheta_1 t} + \Theta_2 e^{\vartheta_2 t}, \tag{14}$$

$$M_{xy,B}(t) = \Theta_3 e^{\vartheta_1 t} + \Theta_4 e^{\vartheta_2 t}, \tag{15}$$

where

$$\vartheta_1 = 1/2\Big\{ -(k_{2A} + k_{2B}) + \sqrt{(k_{2A} - k_{2B})^2 + 4k_A k_B}\Big\}, \tag{16}$$

$$\vartheta_2 = 1/2\Big\{ -(k_{2A} + k_{2B}) - \sqrt{(k_{2A} - k_{2B})^2 + 4k_A k_B}\Big\}, \tag{17}$$

$$\Theta_1 = \Big\{ -(\vartheta_2 + k_{2A})M_{xy,A}^0 + k_B M_{xy,B}^0\Big\}/(\vartheta_1 - \vartheta_2), \tag{18}$$

$$\Theta_2 = \Big\{(\vartheta_1 + k_{2A})M_{xy,A}^0 - k_B M_{xy,B}^0\Big\}/(\vartheta_1 - \vartheta_2), \tag{19}$$

$$\Theta_3 = \Big\{k_A M_{xy,A}^0 + (\vartheta_1 + k_{2A})M_{xy,B}^0\Big\}/(\vartheta_1 - \vartheta_2), \tag{20}$$

$$\Theta_4 = \Big\{ -k_A M_{xy,A}^0 - (\vartheta_2 - k_{2A})M_{xy,B}^0\Big\}/(\vartheta_1 - \vartheta_2) \tag{21}$$

and

$$k_{2A} = R_{2,A} - i\omega_A + k_A,$$

$$k_{2B} = R_{2,B} - i\omega_B + k_B.$$

Furthermore, $M_{xy,j}^0$ is the initial transverse magnetizations of site j, $j = A, B$. If an inversion recovery experiment is performed, as in this study, $M_{xy,j}^0$ is given by $M_{z,j}(\tau)$, where τ is the relaxation delay of the experiment.

It should be noted that both the eigenvalues, ϑ_1 and ϑ_2, and the constants, Θ_1, Θ_2, Θ_3, and Θ_4, are complex numbers. The real parts of ϑ_1 and ϑ_2 correspond to the transverse relaxation rates, while the imaginary parts are the Larmor frequencies. Because of the chemical exchange process, magnetization will be transferred between the two sites A and B during the free induction decay (FID). As shown in Eqs. (14) and (15), the time dependence of $M_{xy,j}(t)$ is bi-exponential. However, the FID is given by the equation

$$\mathrm{FID}(t) = \Theta_1 e^{\vartheta_1 t} + \Theta_2 e^{\vartheta_2 t} + \Theta_3 e^{\vartheta_1 t} + \Theta_4 e^{\vartheta_2 t}, \tag{22}$$

$$= (\Theta_1 + \Theta_3)e^{\vartheta_1 t} + (\Theta_2 + \Theta_4)e^{\vartheta_2 t}, \tag{23}$$

which by Fourier transformation results in two *Lorentzian-line-shape* signals corresponding to the two terms $(\Theta_1 + \Theta_3)e^{\vartheta_1 t}$ and $(\Theta_2 + \Theta_4)e^{\vartheta_2 t}$. Thus, the intensity, the Larmor frequency, the transverse relaxation rate, and the phase of the two signals are given by $|\Theta_1 + \Theta_3|$, and $|\Theta_2 + \Theta_4|$; $\Im(\vartheta_1)$, and $\Im(\vartheta_2)$; $-\Re(\vartheta_1)$, and $-\Re(\vartheta_2)$; and $\arctan(\Im(\Theta_1 + \Theta_3)/\Re(\Theta_1 + \Theta_3))$, and $\arctan(\Im(\Theta_2 + \Theta_4)/\Re(\Theta_2 + \Theta_4))$, respectively. Here $\Re(z)$ and $\Im(z)$ denote the real and the imaginary parts of the complex number z, respectively. However, none of the two signals corresponds exclusively to any of the two exchanging sites, but contain information about both sites and about the exchange rate. As detailed below, this entanglement of the information can give rise to systematic errors in the data analysis, unless it is taken into account.

3.3. Intensity and phase distortions

As shown by Eq. (23), the amplitudes of the two signals A and B are given by $\Theta_1 + \Theta_3$ and $\Theta_2 + \Theta_4$. From Eqs. (18)–(21) it is seen that, in general, the intensities of the two signals are *not* proportional to the molar fractions of the two sites. This discrepancy is most pronounced close to the intermediate exchange regime, $k_A + k_B \lesssim |R_{2,A} - R_{2,B} - i(\omega_a - \omega_b)|$, where two separate signals are observed, although with severe intensity distortions. Furthermore, the amplitudes of the two signals are complex numbers and will, in general, have different phases. However, if separate signals are observed and the slow exchange condition applies, the intensities are to a good approximation proportional to the molar fractions, and phase distortion is absent.

3.4. Implementation of the scalar spin–spin coupling

So far scalar spin–spin coupling has been neglected. In the case of weak coupling, the equations derived above can easily be extended to include spin–spin coupling, if the coupling is the same in the two environments. In this case, the evolution of the transverse magnetization of *each transition* in the multiplet is identical to that described above for an uncoupled signal [17]. Thus, for the same scalar coupling constant, J, in the two sites, and a spin multiplicity of n, the FID takes the form

$$\mathrm{FID}(t) = \big((\Theta_1 + \Theta_3)e^{\vartheta_1 t} + (\Theta_2 + \Theta_4)e^{\vartheta_2 t}\big)\cos^{(n-1)}\pi J t \tag{24}$$

since $\cos z = (1/2)(e^{iz} + e^{-iz})$. The Bloch–McConnell equations do not apply for the exchange of strongly coupled spins, where a more general density matrix description must be used [18].

4. Results and discussion

4.1. Electron self-exchange in A.v. plastocyanin

Plastocyanin from *Anabaena variabilis* and its electron self-exchange (ESE) were employed to illustrate the implications of using approximate solutions of the

Bloch–McConnell equations in the analysis of chemically exchanging systems. During the ESE process, the nuclei exchange between two distinct magnetic environments, the diamagnetic in reduced plastocyanin (*A.v.* PCu(I)) and the paramagnetic in oxidized plastocyanin (*A.v.* PCu(II)), that is

$$\mathrm{PCu(I)} \underset{f_d k_{ese} c}{\overset{f_p k_{ese} c}{\rightleftharpoons}} \mathrm{PCu(II)}, \tag{25}$$

f_p and f_d being the molar fractions of the paramagnetic and the diamagnetic species, respectively. Here $f_p k_{ese} c$ and $f_d k_{ese} c$ correspond to k_A and k_B, respectively, in Eq. (1). Furthermore, the longitudinal and the transverse relaxation rates, and the Larmor frequency in the two environments are R_{1d}, R_{2d}, ω_d, and $R_{1d} + R_{1p}$, $R_{2d} + R_{2p}$, $\omega_d + \omega_p$, respectively, where R_{1p} and R_{2p} are the paramagnetic relaxation enhancements and ω_p is the paramagnetic shift, i.e., the Fermi contact shift and/or the pseudo-contact shift. Both the diamagnetic relaxation and the inhomogeneity line broadening are included in R_{2d}, allowing reliable paramagnetic relaxation enhancements to be obtained from the observed linewidths.

The K20 H^{α} and the V41 H^{γ_1} signals from *A.v.* PCu were chosen for the complete analysis. These signals are both well-resolved in the one-dimensional ^{1}H spectrum, as shown in Fig. 1. The size of the pseudo-contact shift of V41 H^{γ_1} at the applied magnetic field strength, and

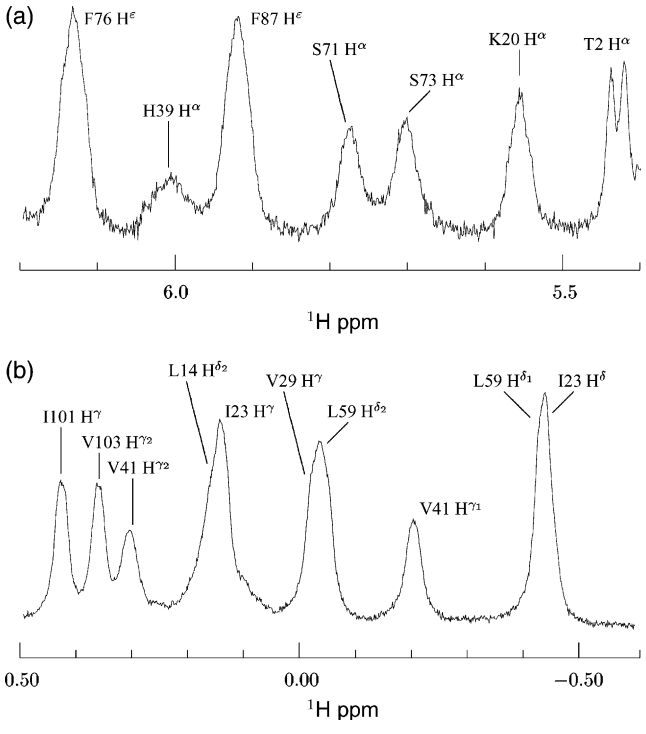

Fig. 1. Regions of the 500 MHz 1D ^{1}H NMR spectrum of *A.v.* PCu: (a) the aromatic region showing the position of the K20 H^{α} and H39 H^{α} resonances; (b) the aliphatic region showing the position of the V41 H^{γ_1} and V41 H^{γ_2} resonances. The molar fraction, f_p, of the oxidized species was 0.094 and the protein concentration was 0.95 mM.

the rate of the ESE process result in a single exchange-averaged signal at the higher protein concentrations, while two separate signals are observed at the lower concentrations. Therefore, not only does the V41 H^{γ_1} resonance illustrate many of the properties of a chemically exchanging system in a clear way. Also, the information that can be obtained from the signal is sufficiently versatile for a complete analysis using the general solution of the Bloch–McConnell equations. In the case of K20 H^{α}, the size of the pseudo-contact shift at the applied magnetic field strength and the rate of the ESE process result in a single exchange-averaged signal at all the applied concentrations. Still, the information that can be obtained from the signal is sufficiently versatile for a complete analysis, allowing a reliable estimation of all the involved parameters. Below it is indicated briefly how the information necessary for the complete analysis can be obtained by varying the ratio of the exchanging species and the exchange rate. Furthermore, it is shown how all the involved parameters can be estimated from a complete analysis of the data, using the general Bloch–McConnell equations.

4.2. Variation of the K20 H^{α} and V41H^{γ_1} signals with the molar fractions of the two sites

In Fig. 2, single exchange-averaged signals of K20 H^{α} and V41 H^{γ_1}, respectively, are shown for different molar fractions, f_p, of the oxidized species and a constant protein concentration. The series of spectra reveals that the K20 H^{α} signal moves downfield, while the V41 H^{γ_1} signal moves upfield with increasing f_p fractions, reflecting opposite signs of the pseudo-contact shift of the two nuclei in the oxidized form. At the applied protein concentration, single exchange-averaged signals are observed in all cases, i.e., the Larmor frequency of the observed signals is to a first order of approximation given by a weighted average of the frequencies of the two sites (see discussion below). Furthermore, as the fraction of the oxidized species is increased, the linewidth of the resonances increases because of the exchange process, the pseudo-contact shift, and the larger transverse relaxation rate in the oxidized species caused by the paramagnetic relaxation enhancement. Consequently, the obtained spectra depend on most of the involved parameters.

4.3. Variation of the V41 H^{γ_1} signal with the ESE rate

Additional, independent information about the NMR parameters is obtained from the variation of the resonances with the ESE rate, $k_{ese}c$. Thus, by decreasing the protein concentration and thereby lowering the ESE rate, an extra V41 H^{γ_1} signal appears approximately 65 Hz upfield from the original signal, as shown in Fig. 3. The new signal is the paramagnetic shifted signal of

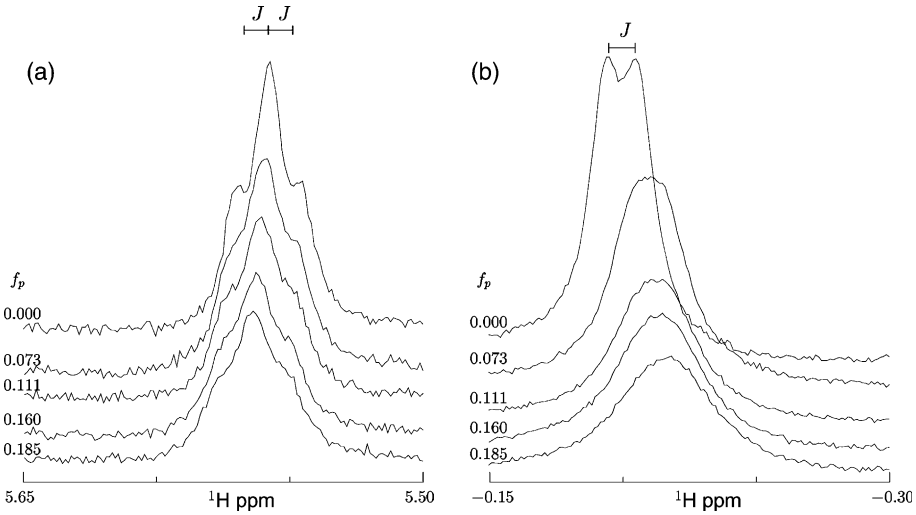

Fig. 2. The resonances of (a) K20 H^{α} and (b) V41 H^{γ_1} in *A.v.* PCu recorded at 500 MHz. The protein concentration was 1.89 mM, while the molar fraction, f_p, of the oxidized species was varied as shown to the left in the two figures. A line broadening caused by the electron self-exchange, the R_{2p} relaxation, and the pseudo-contact shift is clearly observed. The triplet splitting observed for K20 H^{α} at $f_p = 0$ is caused by the scalar spin–spin coupling between the H^{α} proton and the H^{β} protons. The doublet splitting observed for V41 H^{γ_1} is caused by the scalar spin–spin coupling between the H^{γ_1} protons and the H^{β} proton.

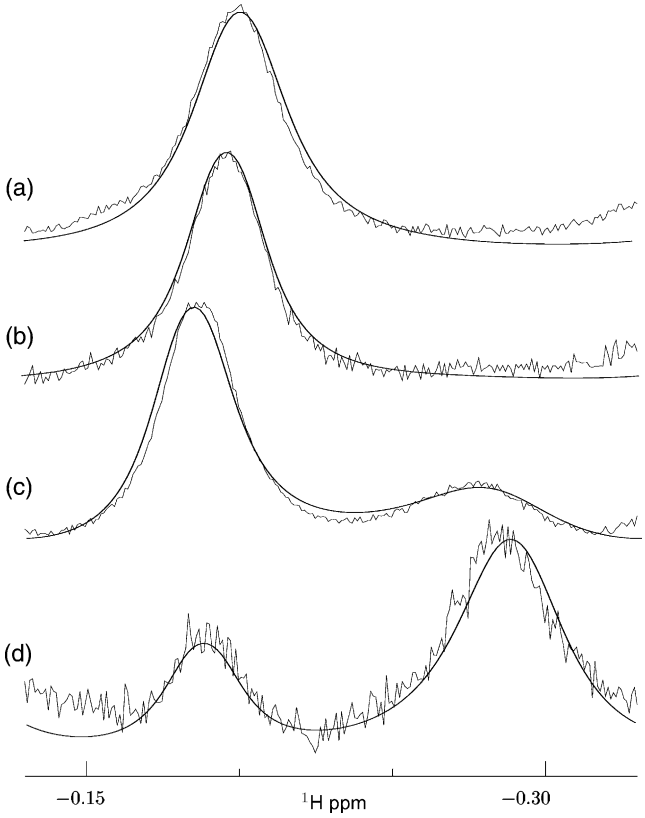

Fig. 3. The resonances of V41 H^{γ_1} in *A.v.* PCu recorded at 500 MHz, for different molar fractions, f_p, of the oxidized species and different protein concentrations. (a) $f_p = 0.19$ and $c = 1.89$ mM; (b) $f_p = 0.16$ and $c = 0.95$ mM; (c) $f_p = 0.37$ and $c = 0.53$ mM; (d) $f_p = 0.80$ and $c = 0.08$ mM. Two separate signals appear when the concentration is decreased. The noiseless signals were obtained by Fourier transformation of simulated FIDs consisting of 256 complex points. The simulated FIDs were generated from the general solution, Eq. (24), using the parameters listed in Table 2.

V41 H^{γ_1}, as suggested by a fit of the simplest approximation, $v = v_d + f_p v_p$, to the variation of the frequency with f_p at the highest protein concentration (Fig. 2), and by the *g*-tensor components of spinach plastocyanin [19]. This was definitively confirmed by the observation of a correlation between the two signals in the TOCSY spectrum. The fit gives a pseudo-contact shift of -35.5 ± 0.9 Hz, while the *g*-tensor components together with the position of V41 H^{γ_1} in the principal coordinate system of the *g*-tensor predict a pseudo-contact shift of -87 Hz, assuming an axial symmetric *g*-tensor with the principal axis aligned along the Cu(II)–M97 S^{δ} bond.

4.4. The complete analysis

The data analysis was based on the one-dimensional, non-selective R_1 experiments listed in Table 1. The experiments were recorded on samples with different protein concentrations, *c*, and different oxidation degree, f_p. The linear prediction model method was used for the analysis, as described in Section 2. However, it should be emphasized that any computational approach that can extract the spectral parameters from the experimental data in a reliable way can be used.

The total set of auxiliary FIDs derived from the R_1 experiments was analyzed simultaneously, using the general solution of the Bloch–McConnell equations, Eq. (24). Thus the paramagnetic relaxation enhancements, R_{1p} and R_{2p}, and the pseudo-contact shift, ω_p, for the K20 H^{α} proton and the V41 H^{γ_1} protons were estimated from the 11×22 and 11×27 FIDs, respectively, together with the k_{ese} rate constant. In addition, an initial magnetization, M_z^0, an equilibrium magnetization, M_z^{∞},

Table 1
Experiments and *A.v.* PCu samples used in the complete analysis[a]

	Conc. (mM)	f_p[b]
Exp. 1	1.89	0.07
Exp. 2	1.89	0.11
Exp. 3	1.89	0.16
Exp. 4	1.89	0.19
Exp. 5	0.95	0.01
Exp. 6	0.95	0.05
Exp. 7	0.95	0.09
Exp. 8	0.95	0.12
Exp. 9	0.95	0.16
Exp. 10	0.53	0.09
Exp. 11	0.53	0.10
Exp. 12	0.53	0.23
Exp. 13	0.53	0.36
Exp. 14	0.53	0.50
Exp. 15	0.53	0.62
Exp. 16	0.47	0.01
Exp. 17	0.47	0.04
Exp. 18	0.47	0.08
Exp. 19	0.47	0.10
Exp. 20	0.47	0.18
Exp. 21	0.48	0.19
Exp. 22	0.49	0.25
Exp. 23[c]	0.08	0.08
Exp. 24[c]	0.08	0.28
Exp. 25[c]	0.08	0.80
Exp. 26[c]	0.08	0.75
Exp. 27[c]	0.08	0.92

[a] Using the general solution of the Bloch–McConnell equations, Eq. (24).
[b] The fractions of the oxidized species of *A.v.* PCu.
[c] Not used in the complete analysis of K20 H^{α} because of overlap in the spectrum.

and a phase, ϕ, were estimated for each of the R_1 experiments. Furthermore, the relaxation rates, R_{1d} and R_{2d}, and the chemical shift of the diamagnetic site were estimated at all the applied concentrations, resulting in a total of 83 (K20 H^{α}) and 101 (V41 H^{γ_1}) parameters estimated in the analysis. The initial transverse magnetization, $M^0_{xy,j}$, in Eq. (24) (and Eqs. (18)–(21)) was calculated from the longitudinal magnetization Eqs. (4)–(11), assuming an ideal 90° exitation pulse, that is, $M^0_{xy,j} = M_{z,j}(\tau)$. Because of the chemical equilibrium between the oxidized and reduced *A.v.* PCu, the following relations apply and were used:

$$M^0_{z,p} = f_p M^0_z, \quad M^0_{z,d} = f_d M^0_z, \tag{26}$$

$$M^{\infty}_{z,p} = f_p M^{\infty}_z \quad M^{\infty}_{z,d} = f_d M^{\infty}_z, \tag{27}$$

where $M^0_{z,p}$ and $M^0_{z,d}$ are the initial, longitudinal magnetizations of the paramagnetic and diamagnetic sites, respectively, while $M^{\infty}_{z,p}$ and $M^{\infty}_{z,d}$ are the corresponding equilibrium magnetizations, and M^0_z and M^{∞}_z are the total initial and equilibrium longitudinal magnetizations, respectively. The parameters describing the paramagnetic site and the exchange rate constant, that were obtained in the complete analysis, are shown in Table 2. The uncertainties given in Table 2 are those obtained in the least-squares fit. The absolute uncertainties (0.002–0.02) of the experimental f_p fractions were neglected in the data analysis. Therefore, the true uncertainties of the parameters are slightly larger than those shown in Table 2.

4.5. The reliability of the parameters obtained in the complete analysis

Spectra that are simulated from the estimated parameters using Eq. (24), are in good agreement with the experimental spectra, as shown in Figs. 3 and 4. Thus, the estimated parameters and the general solution of the Bloch–McConnell equations account well for the experimental spectra. Further support of the reliability of the estimated parameters is provided by the consistencies of the electron self-exchange rates, k_{ese}, obtained from the two signals, V41 H^{γ_1} and K20 H^{α}, and by the electron relaxation rate, and the physically meaningful Cu^{2+}–V41 H^{γ_1} and Cu^{2+}–K20 H^{α} distances that can be derived from the obtained R_{1p} and R_{2p} rate constants, as discussed below.

4.6. Information on A.v. plastocyanin from the complete analysis

The electron relaxation rate and the distance between the nuclei and the paramagnetic metal ion can be determined from the R_{1p} and R_{2p} rate constants. This holds, if both relaxation rates are pure dipolar, and if the observed differences in relaxation rates between the reduced and the oxidized protein are caused only by the paramagnetic enhancement. The Curie spin relaxation can be neglected in blue copper proteins because of the slow electron relaxation rate [20,21]. Thus, assuming

Table 2
Parameters obtained in the complete analysis[a]

	R_{1p} (s^{-1})	R_{2p} (s^{-1})	ν_p (Hz)	k_{ese} ($mM^{-1}s^{-1}$)
K20 H^{α}	1.75 ± 0.10	2.77 ± 0.32	23.59 ± 0.54	214.5 ± 5.5
V41 H^{γ_1}	18.77 ± 0.22	37.9 ± 0.9	-64.82 ± 0.18	222.4 ± 2.5

[a] A least-squares analysis using the general solution of the Bloch–McConnell equations, Eq. (24). The analysis included a simultaneous fit to 11×22 auxiliary FIDs of the K20 H^{α} signal and 11×27 auxiliary FIDs of the V41 H^{γ_1} signals of *A.v.* PCu, as described in Section 2. The experiments used in the least-squares analysis are listed in Table 1.

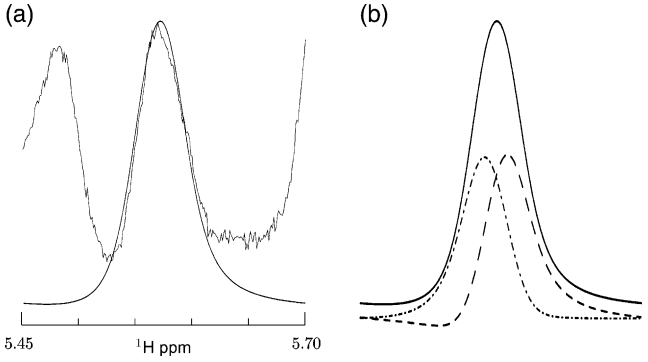

Fig. 4. The resonance of K20 H^{α} in *A.v.* PCu recorded at 500 MHz. The molar fraction, f_p, of the oxidized species was 0.50 and the concentration of the protein was 0.54 mM. (a) Comparison of the experimental spectrum of K20 H^{α} and a simulated spectrum (noiseless signal). The simulated spectrum was obtained by Fourier transformation of a simulated FID consisting of 256 complex points and the simulated FID was generated from the general solution, Eq. (24), using the parameters obtained in the least-squares analysis, listed in Table 2. In (b) is shown how the simulated spectrum in (a) is composed of two signals. Here (– – –) correspond to the term $(\Theta_1 + \Theta_3)e^{\vartheta_1}$ and (– · –) corresponds to the term $(\Theta_2 + \Theta_4)e^{\vartheta_2}$ of Eq. (24). It is noted that the two subpeaks have different phases.

that the point dipole approximation applies, electron relaxation rates of $3.8 \pm 1.0 \times 10^9$ and $2.6 \pm 0.2 \times 10^9$ s^{-1} were calculated from the paramagnetic relaxation enhancements of K20 H^{α} and V41 H^{γ_1}, respectively. More specifically, the effective correlation time was calculated from the ratio of the two paramagnetic relaxation enhancements in Table 2, using the Solomon equations for pure dipolar relaxation [22].

$$\frac{R_{2p}}{R_{1p}} = \frac{7}{6} + \frac{2}{3}\omega_I^2\tau_{c,1}^2. \tag{28}$$

Here ω_I is the Larmor frequency of the nucleus and $\tau_{c,1}$ is the effective correlation time corresponding to $\tau_{c,1}^{-1} = R_{1e} + \tau_R^{-1}$, where R_{1e} is the longitudinal relaxation rate of the unpaired electron and τ_R the rotational correlation time of the protein. Furthermore, a Cu^{2+}–K20 H^{α} distance of 13.7 ± 0.2 Å (14.7 Å) and a Cu^{2+}–V41 H^{γ_1} distance of 9.25 ± 0.02 Å (8.95 Å) were obtained from the paramagnetic relaxation enhancements in Table 2. The distances were calculated from either one of the two individual relaxation enhancements, using the corresponding Solomon equation. The distances in the brackets are those measured in the NMR solution structure of the protein [3].

The electron relaxation rates obtained here deviate by more than the experimental errors from the electron relaxation rate, $5.8 \pm 0.5 \times 10^9\,s^{-1}$ found previously for *A.v.* PCu(II), using the field dependence of the R_{1p} rates [2]. The deviation is most pronounced for the V41 H^{γ_1} protons, and may reflect the mobility of the side chain of V41. A mobility of the side chain on the millisecond time scale will increase the effective transverse relaxation rate of the V41 H^{γ_1} protons. Since this contribution to the relaxation is not included in the applied model for the R_{2p} relaxation, it results in an apparent increase of the calculated R_{2p} rate, and thereby in an underestimation of the electron relaxation rate when calculated from the R_{1p} and R_{2p} relaxation rates obtained here using Eq. (28). The electron relaxation rate obtained from the paramagnetic relaxation enhancements of K20 H^{α} is in better agreement with the value obtained previously [2]. This indicates that the millisecond–microsecond time scale motion of K20 H^{α} is less pronounced than the motion of V41 H^{γ_1}, in accordance with the location of K20 H^{α} in the backbone of the protein. Still, the mobility of K20 H^{α} is in agreement with recent model-free relaxation studies of the backbone dynamics of the protein [23], which indicate a millisecond–microsecond time scale motion of the adjacent backbone K20 ^{15}N nucleus.

All taken together, the estimation of an electron relaxation rate using Eq. (28) that is too small suggests a millisecond–microsecond time scale motion of both the V41 side chain and the K20 H^{α} proton. However, the results here do not indicate whether this flexibility is unique for the oxidized form of the protein, since a similar flexibility in the reduced form will have only little influence on the relaxation rates because of the missing paramagnetic interaction with the metal ion.

4.7. The approximate solutions of the Bloch–McConnell equations; the fast exchange condition

As shown by Eqs. (14) and (15), the evolution of the transverse magnetization is given by the transverse relaxation rate and the Larmor frequency. If the pseudo-first order exchange rate, $k_{ese}c$, is large compared with the paramagnetic shift, ω_p, and the difference in transverse relaxation rate, R_{2p}, only a single exchange-averaged NMR signal is observed at an intermediate frequency. More specifically, this so-called fast exchange condition is fulfilled when the following inequality applies [8]:

$$k_{ese}c \gg |R_{2p} - i\omega_p|. \tag{29}$$

In the fast exchange regime, the amplitude of the exponential terms in Eqs. (14) and (15) that involves ϑ_2 is negligible, i.e., $|\Theta_1 + \Theta_3| \gg |\Theta_2 + \Theta_4|$. This can be concluded from the general solution, Eq. (24), where the ratio of the two amplitudes, $\Theta_1 + \Theta_3$ and $\Theta_2 + \Theta_4$, is given by

$$\frac{\Theta_2 + \Theta_4}{\Theta_1 + \Theta_3} \simeq \frac{M_{xy,d}^0(f_p x + f_d f_p x^2) - M_{xy,p}^0(f_d x - f_d f_p x^2)}{M_{xy,d}^0(1 - f_d x + f_d f_p x^2) + M_{xy,p}^0(1 + f_p x + f_d f_p x^2)} \tag{30}$$

and

$$x = \frac{R_{2p} - i\omega_p}{k_{ese}c}$$

assuming that the fast exchange condition applies. From Eq. (30) it is clear that $|\Theta_1 + \Theta_3| \gg |\Theta_2 + \Theta_4|$ under the fast exchange condition where $|x| \ll 1$. This results in the observation of a single exchange-averaged signal in the spectrum instead of two separate signals. The Larmor frequency and the transverse relaxation rate of the exchange-averaged signal are to a second order of approximation given by

$$R_2 = -\Re(\vartheta_1) \simeq R_{2d} + f_p R_{2p} - \frac{f_p(1-f_p)}{k_{ese}c}\left(R_{2p}^2 - \omega_p^2\right) + \cdots, \quad (31)$$

$$\omega = \Im(\vartheta_1) \simeq \omega_d + f_p\omega_p - \frac{2f_p(1-f_p)}{k_{ese}c}\omega_p R_{2p} + \cdots. \quad (32)$$

Normally, it is assumed that the fast exchange condition, Eq. (29), is fulfilled if a single exchange-averaged signal is observed. However, if the transverse relaxation rate in one of the two sites is sufficiently high, one of the signals may be broadened beyond detection and only one signal is observed, even though the fast exchange condition is not fulfilled. Also, if the populations in the two sites are very different only one signal is observed, irrespective of the lack of fulfillment of the fast exchange condition. In the present study, it is primarily the first mentioned condition that applies.

In Fig. 3, a single exchange-averaged signal is observed for V41 H^{γ_1} at *A.v.* PCu concentrations of 1.89 and 0.95 mM, i.e., apparently the resonance is in the fast exchange regime where the approximate expressions, Eqs. (31) and (32), apply. However, the plots in Figs. 5 and 6 based on the parameters obtained in the complete analysis clearly show that these approximate solutions are not valid, even at the highest concentration. In the same way, a single exchange-averaged signal is observed for K20 H^{α} at *A.v.* PCu concentrations of 1.89, 0.95, and 0.54 mM, as shown in Figs. 1, 2, and 4, while the plots in Fig. 7, that are based on the parameters obtained in the complete analysis, clearly reveal that the approximate solutions are not valid. Nevertheless, if the simplest approximate solutions of the Bloch–McConnell equations for the fast exchange case, i.e., $R_2 = R_{2d} + f_p R_{2p}$ and $v = v_d + f_p v_p$, are used to analyze the paramagnetic line broadenings and frequency shifts shown in Figs. 5–7, excellent fits are obtained. However, the apparent pseudo-contact shifts, v_p, and paramagnetic transverse relaxation enhancements, R_{2p}, that are derived (Table 3), deviate substantially from the corresponding values obtained in the complete analysis, Table 2. Moreover, the deviations increase as the concentration decreases. Therefore, none of the two resonances V41 H^{γ_1} and K20 H^{α} are in the fast exchange regime, even though single exchange-averaged signals are observed. Consequently, erroneous results are obtained if the simplest approximate solution is used in the data analysis despite the fact that it might fit the data, as demonstrated here. For K20 H^{α} a simultaneous fit of the second order approximations, Eqs. (31) and (32), is possible and results in $v_p = 22.4 \pm 3.9$ Hz, $k_{ese} = 216 \pm 28$ mM, and $R_{2p} = -25 \pm 20$ s^{-1}. Here, the pseudo-contact shift, v_p, and the electron self-exchange rate constant are in good agreement with the parameters obtained in the complete analysis, Table 3. However a non-physical R_{2p} rate is obtained. In the case of V41 H^{γ_1} the second order approximation cannot be fitted to the experimental data in Figs. 5 and 6, since the signal is too far from the fast exchange regime. Therefore, no information about the exchange

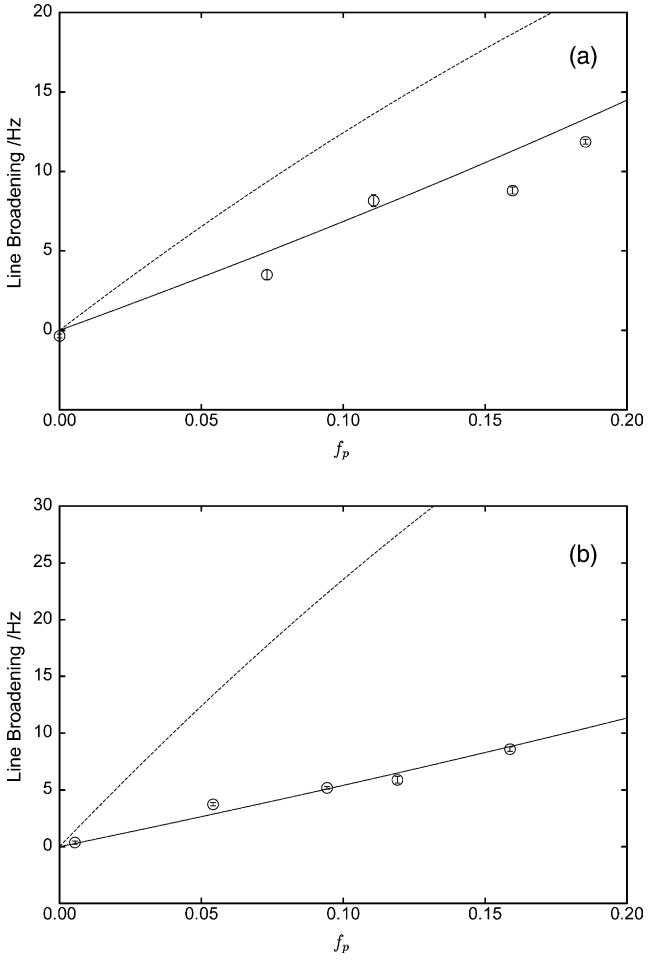

Fig. 5. The observed line broadening of the exchange-averaged signal of V41 H^{γ_1} in *A.v.* PCu recorded at 500 MHz and two different protein concentrations: (a) $c = 1.89$ mM, (b) $c = 0.95$ mM and with different molar fractions, f_p, of the oxidized species. The full-drawn lines correspond to the least-squares fit of the general solution, i.e., the real part, $\Re(\vartheta_1)$, of Eq. (16). The dashed line corresponds to the approximate solution, Eq. (31), and was calculated using the parameters obtained in the complete analysis by the least-squares fit of the general solution. The deviation between the two curves clearly shows that the approximate solution does not apply even though a single exchange-averaged signal is observed in the spectra (Figs. 2 and 3a, b) and the linewidth of the signal depends linearly on f_p.

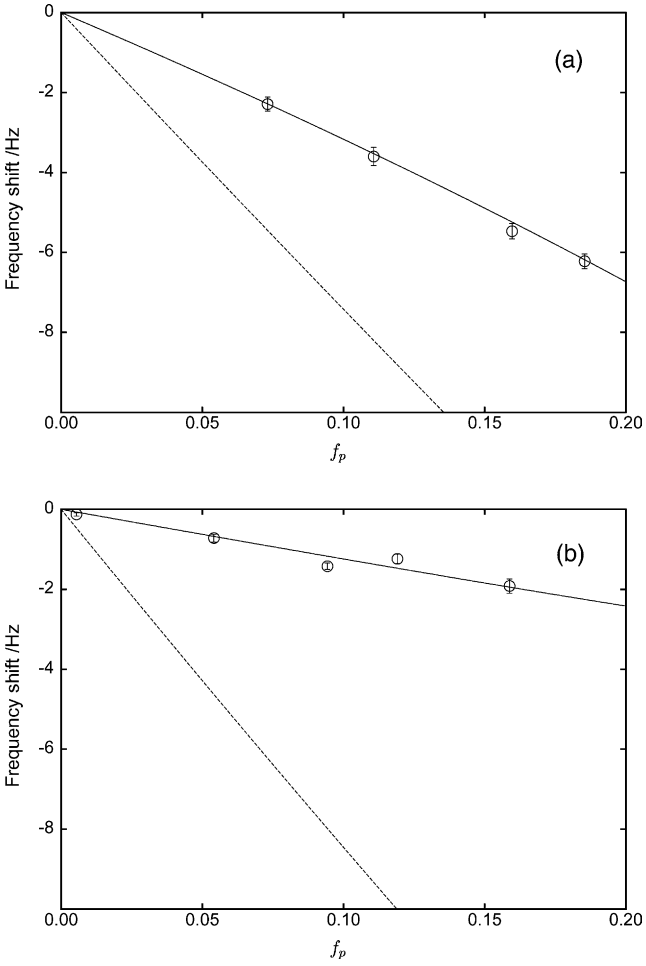

Fig. 6. The observed frequency shift of the exchange-averaged signal of V41 H^{γ_1} in *A.v.* PCu recorded at 500 MHz and two different protein concentrations: (a) $c = 1.89$ mM, (b) $c = 0.95$ mM and with different molar fractions, f_p, of the oxidized species. The full-drawn line corresponds to the least-squares fit of the general solution, i.e., the imaginary part, $\Im(\vartheta_1)$, of Eq. (16). The dashed line corresponds to the approximated solution, Eq. (32). The deviation between the two curves clearly shows that the approximated solution does not apply, even though a single exchange-averaged signal is observed in the spectra (Figs. 2 and 3) and the frequency shift depends linearly on f_p.

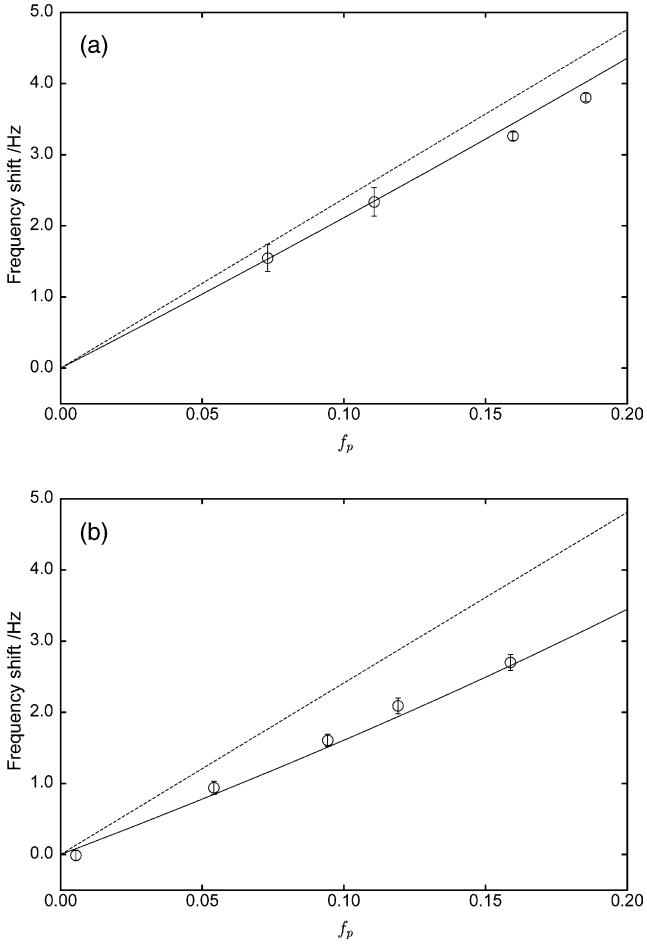

Fig. 7. The observed frequency shift of the exchange-averaged signal of K20 H^{α} in *A.v.* PCu recorded at 500 MHz and two different protein concentrations: (a) $c = 1.89$ mM, (b) $c = 0.95$ mM and with different molar fractions, f_p, of the oxidized species. The full-drawn line corresponds to the least-squares fit of the general solution, i.e., the imaginary part, $\Im(\vartheta_1)$, of Eq. (16). The dashed line corresponds to the approximated solution, Eq. (32). The deviation between the two curves clearly shows that the approximated solution does not apply, even though a single exchange-averaged signal is observed in the spectra (Fig. 2) and the frequency shift depends linearly on f_p.

rate constant k_{ese} can be obtained from the V41 H^{γ_1} signal, using the two highest concentrations and the approximate solution, even though the experimental data clearly depend on k_{ese}.

4.8. The approximate solutions of the Bloch–McConnell equations; the slow exchange condition

If the pseudo-first order exchange rate, $k_{ese}c$, is small compared with the paramagnetic shift, ω_p, and the difference in transverse relaxation rate, R_{2p}, two separate NMR signals are observed in the spectrum. This so-called slow exchange condition is fulfilled when the following inequality applies [8]:

$$k_{ese}c \ll |R_{2p} - i\omega_p|. \tag{33}$$

The transverse relaxation rate and the Larmor frequency of the signal, which approach those of the diamagnetic signal for $k_{ese}c \to 0$, is to a second order of approximation given by

$$R_2 = -\Re(\vartheta_1) \simeq R_{2d} + f_p k_{ese} c - \frac{f_p f_d k_{ese}^2 c^2 R_{2p}}{R_{2p}^2 + \omega_p^2} + \cdots. \tag{34}$$

$$\omega = \Im(\vartheta_1) \simeq \omega_d + \frac{f_p f_d k_{ese}^2 c^2 \omega_p}{R_{2p}^2 + \omega_p^2} + \cdots. \tag{35}$$

Similar equations hold for the signal, which approaches the paramagnetic signal for $k_{ese}c \to 0$.

For V41 H^{γ_1} two separate signals are observed at the lowest protein concentrations. Consequently, the

Table 3
Parameters obtained using the Bloch–McConnell equations

Nucleus	Method	k_{ese} ($mM^{-1}s^{-1}$)	R_{2p} (s^{-1})	ν_p (Hz)
K20 H^{α}	Complete[a]	214.5 ± 5.5	2.8 ± 0.3	23.6 ± 0.5
	Fast exch.[b,c]	—	14 ± 3	20.1 ± 0.4
	Fast exch.[b,d]	—	18 ± 2	17.9 ± 0.4
	Fast exch.[e]	216 ± 28	-25 ± 20	22.4 ± 3.9
V41 H^{γ_1}	Complete[a]	222.4 ± 2.5	37.9 ± 0.9	-64.82 ± 0.18
	Fast exch.[b,c]	—	64 ± 4	-35.5 ± 0.9
	Fast exch.[b,d]	—	52 ± 4	-12.2 ± 1.4
	Slow exch.[f]	220 ± 27	194 ± 160	-55 ± 16
V41 H^{γ_2}	Slow exch.[g]	220.4 ± 8.9	—	—
H39 H^{α}	Slow exch.[g]	246 ± 17	—	—

[a] The general solution Eq. (24) was used, see Table 2.
[b] The fast exchange condition was assumed and the simplest approximate solutions were used, i.e., $R_2 = R_{2d} + f_p R_{2p}$ and $\nu = \nu_d + f_p \nu_p$ ($\nu = \omega/2\pi$), see Figs. 5–7.
[c] Only data obtained at a protein concentration of 1.89 mM were used.
[d] Only data obtained at a protein concentration of 0.95 mM were used.
[e] A simultaneous least-squares fit of Eqs. (31) and (32) to the line broadenings and frequency shifts obtained at protein concentrations of 1.89 and 0.95 mM.
[f] A simultaneous least-squares fit of Eqs. (34) and (35) to the line broadenings and frequency shifts obtained at protein concentrations of 0.95, 0.54, 0.47, and 0.08 mM, see Fig. 8.
[g] The slow exchange condition was assumed and the simplest approximate solutions were used, i.e., $R_2 = R_{2d} + f_p k_{ese} c$, see Figs. 9 and 10.

nucleus is close to the slow exchange regime and, according to Eqs. (34) and (35), information about the exchange rate, k_{ese}, the pseudo-contact shift, ω_p, and the paramagnetic relaxation enhancement, R_{2p}, can, in principle, be obtained from the line broadening and the frequency shifts of *only one of the signals*, using these equations. In Fig. 8 is shown a simultaneous least-squares fit of Eqs. (34) and (35) to the line broadening and frequency shifts of the V41 H^{γ_1} signal obtained at four different protein concentrations, 0.95, 0.54, 0.47, and 0.08 mM. The results are given in Table 3. The obtained electron self-exchange rate, $k_{ese} = 220 \pm 27\,mM^{-1}s^{-1}$, and the pseudo-contact shift, $\nu_p = -55 \pm 16$ Hz, are in good agreement with the results derived in the complete analysis, Table 2. However, also in this case the paramagnetic relaxation enhancement remains practically undetermined ($R_{2p} = 194 \pm 160\,s^{-1}$ versus $37.9 \pm 0.9\,s^{-1}$ in the complete analysis).

If the line broadening depends linearly on cf_p, the observed relaxation rate, R_2, is independent of the pseudo-contact shift and the paramagnetic relaxation enhancement, and no information about these

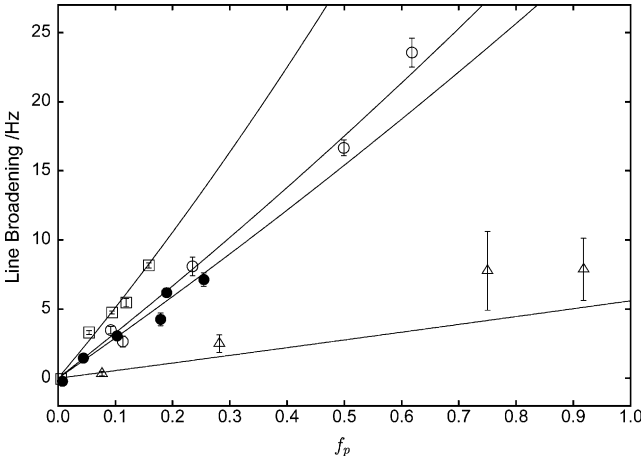

Fig. 8. The observed line broadening of the exchange-averaged signal of V41 H^{γ_1} in *A.v.* PCu recorded at 500 MHz and at different protein concentrations: (□) $c = 0.95$ mM, (○) $c = 0.54$ mM, (●) $c = 0.47$ mM, and (△) $c = 0.08$ mM. The full-drawn line corresponds to a simultaneous least-squares fit of the approximate solutions, Eq. (34) and (35), to the observed line broadening and frequency shift. The parameters obtained in the least-squares fit are $k_{ese} = 220 \pm 27\,mM^{-1}s^{-1}$, $R_{2p} = 194 \pm 160\ s^{-1}$, and $\nu_p = -55 \pm 16$ Hz.

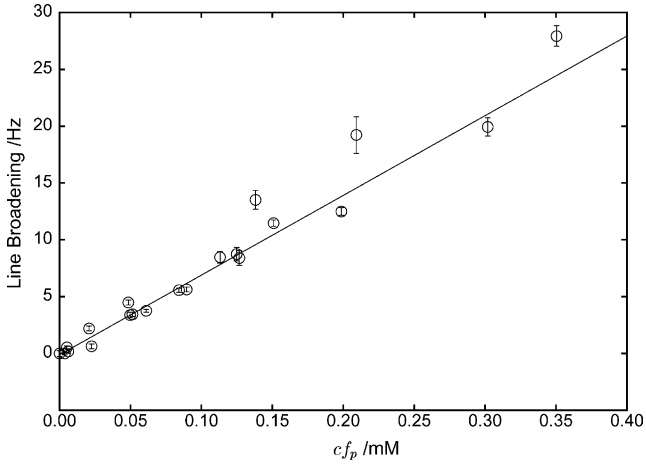

Fig. 9. The observed line broadening of the exchange-averaged signal of V41 H^{γ_2} in *A.v.* PCu recorded at 500 MHz. The line broadening is shown for different protein concentrations, c, and different molar fractions, f_p, of the oxidized species. The full-drawn line corresponds to a linear least-squares fit of Eq. (36) to the data shown. The line broadening depends linearly on $f_p c$, indicating that the slow exchange condition is fulfilled and that the exchange rate can be obtained from the linear least-squares fit ($k_{ese} = 220.4 \pm 8.9\,mM^{-1}\,s^{-1}$) (see text).

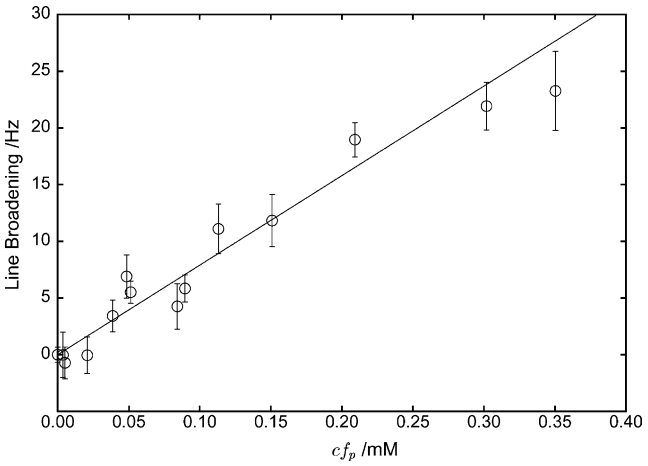

Fig. 10. The observed line broadening of the exchange-averaged signal of H39 H^{α} in *A.v.* PCu recorded at 500 MHz. The line broadening is shown for different protein concentrations, c, and different molar fractions, f_p, of the oxidized species. The full-drawn line corresponds to a linear least-squares fit of Eq. (36) to the data shown. The line broadening depends linearly on $f_p c$, indicating that the slow exchange condition is fulfilled and that the exchange rate can be obtained from the linear least-squares fit ($k_{ese} = 246 \pm 17\,mM^{-1}\,s^{-1}$) (see text).

parameters can be obtained. Still, the first order approximation corresponding to Eq. (34)

$$R_2 = R_{2d} + f_p k_{ese} c \tag{36}$$

can be used to gain information on the exchange rate, k_{ese}. This holds for the line broadenings of V41 $H^{\gamma 2}$ and H39 H^{α}, as shown in Figs. 9 and 10, respectively. In these cases, a least-squares analysis of the dependence of the experimental R_2 rates on cf_p using Eq. (36) gives the electron self-exchange rates, k_{ese}, of 220.4 ± 8.9 and $246 \pm 17\,mM^{-1}s^{-1}$, respectively, in good agreement with the results obtained in the complete analysis. Therefore, in the slow exchange limit where the line broadening depends linearly on cf_p, accurate information about the exchange rate can be obtained using Eq. (36).

5. Conclusion

The analysis clearly shows that the observation of a single exchange-averaged signal is not sufficient evidence for the fulfillment of the fast exchange condition for the transverse magnetization, Table 3. Thus, using the simplest approximations will result in paramagnetic relaxation enhancements that are non-physical and inconsistent with the structure, in contrast to the results obtained from the complete analysis. However, information on the exchange rate, k_{ese}, and the pseudo-contact shift, ω_p, can be obtained if more than one protein concentration is used, and if second order approximations of the Bloch–McConnell equations are applied instead of the simplest approximate solutions. Therefore, the simplest approximate solutions of the Bloch–McConnell equations in the fast exchange regime should be used only if it is known a priori that the fast exchange condition is fulfilled. Variation of the exchange rate, here determined by the protein concentration, can reveal whether the fast exchange condition is fulfilled.

In the slow exchange regime, accurate information about the exchange rate can be obtained, if the line broadening depends linearly on cf_p and if no frequency shifts are observed. Furthermore, reliable pseudo-contact shifts can be determined, if the signal is close to the slow exchange regimes, and if second order approximate solutions are used. However, reliable information about the paramagnetic relaxation enhancement is not available in the slow exchange regime, even if second order approximations of the Bloch–McConnell equations are used. In contrast, the general solution accounts well for the observed line broadening and the observed frequency shift, independent of the fulfillment of any approximations, as demonstrated above.

Finally, the complete analysis here shows that a least-squares analysis of a sufficiently versatile set of experimental data using the general solution of the macroscopic Bloch–McConnell equations allows an accurate determination of all the parameters that describe a chemically exchanging system. Thus, using plastocyanin from *Anabaena variabilis* and the electron self-exchange of this metallo-protein as an example, the complete analysis provides an accurate determination of the pseudo-contact shift, ω_p, and the paramagnetic relaxation rates, R_{1p} and R_{2p}, of the K20 H^{α} and V41 $H^{\gamma 1}$ protons of the oxidized form of this protein, as well as the ESE rate constant.

The high reliability of the parameters obtained in the complete analysis is demonstrated not only by the quality of the least-squares fit and the precision of the obtained parameters. It is also evident from the physical meaningful Cu^{2+}–K20 H^{α} and Cu^{2+}–V41 $H^{\gamma 1}$ distances and the electron relaxation rates that were estimated from the R_{1p} and R_{2p} relaxation rates. Thus, the obtained distances are in good agreement with the corresponding distances in the NMR solution structure of *A.v.* PCu [3]. The apparent disagreement of the estimated electron relaxation rates with the rate obtained previously [2] can be accounted for by the flexibility of the protons, especially in the case of the side chain of the V41 residue in the oxidized form.

Acknowledgments

We are grateful to Søren M. Kristensen, Malene R. Jensen, Henrik Gesmar, and Georg Ole Sørensen for helpful discussions, to Jens Ulstrup and Hans E. M. Christensen for providing the *A.v.* PCu samples, and to Lise-Lotte Jespersen and Else Philipp for technical assistance. This work was financially supported by the

Danish Natural Science Research Council (J. Nos. 9400351, 9801801, and 21-01-0545), Direktør Ib Henriksens Fond, Carlsbergfondet and Novo Nordisk Fonden. DFH thanks Novo Nordisk and Novozymes for a Novo Scholarship.

References

[1] D.G.A. Harshani de Silva, D. Beoku-Betts, P. Kyritsis, K. Govindaraju, R. Powls, N.P. Tomkinson, A.G. Sykes, Protein–protein cross-reactions involving plastocyanin, cytochrome f and azurin: self-exchange rate constant and related studies with inorganic complexes, J. Chem. Soc. Dalton Trans. (1992) 2145–2151.

[2] L. Ma, J.J. Led, Determination by high field NMR spectroscopy of the longitudinal electron relaxation rate in Cu(II) plastocyanin from *Anabaena variabilis*, J. Am. Chem. Soc. 122 (2000) 7823–7824.

[3] L. Ma, A.-M.M. Jørgensen, G.O. Sørensen, J. Ulstrup, J.J. Led, Elucidation of the paramagnetic R_1 relaxation of heteronuclei and protons in Cu(II) Plastocyanin from *Anabaene variabilis*, J. Am. Chem. Soc. 122 (2000) 9473–9485.

[4] L. Ma, E. Philipp, J.J. Led, Determination of the electron self-exchange rate of blue copper proteins by super-WEFT spectroscopy, J. Biomol. NMR 19 (2001) 199–208.

[5] M.R. Jensen, D.F. Hansen, J.J. Led, A general method for determining the electron self-exchange rates of blue copper proteins by longitudinal NMR relaxation, J. Am. Chem. Soc. 124 (2002) 4093–4096.

[6] F. Bloch, Nuclear induction, Phys. Rev. 70 (1946) 460–474.

[7] H.M. McConnell, Reaction rates by nuclear magnetic resonance, J. Chem. Phys. 28 (1958) 430–431.

[8] A.C. McLaughlin, J.S. Leigh Jr., Relaxation times in systems with chemical exchange: approximate solutions for nondilute case, J. Magn. Reson. 9 (1973) 296–304.

[9] O. Trott, A.G. Palmer, R_ρ Relaxation outside of the fast-exchange limit, J. Magn. Reson. 154 (2002) 157–160.

[10] U. Badsberg, A.-M.M. Jørgensen, H. Gesmar, J.J. Led, J.M. Hammerstad, L.-L. Jespersen, J. Ulstrup, Solution structure of reduced plastocyanin from the blue-green alga *Anabaena variabilis*, Biochemistry 35 (1996) 7021–7031.

[11] D.S. Wishart, B.D. Sykes, Chemical shifts as a tool for structure determination, Meth. Enzymol. 239 (1994) 363–392.

[12] R. Moss, H. Gesmar, J.J. Led, A new linear prediction model method for the determination of slow amide proton exchange rates from series of one-dimensional ^{1}H NMR spectra, J. Am. Chem. Soc. 116 (1994) 747–749.

[13] D.F. Hansen, J.J. Led, Measuring the longitudinal NMR relaxation rates of fast relaxing nuclei using a signal eliminating relaxation filter, J. Magn. Reson. 151 (2001) 339–346.

[14] H. Gesmar, P.C. Hansen, "Fast" linear prediction and its application to NMR spectroscopy, J. Magn. Reson. A 106 (1994) 236–240.

[15] J.S. Leigh Jr., Relaxation times in systems with chemical exchange: some exact solutions, J. Magn. Reson. 4 (1971) 308–311.

[16] J.J. Led, H. Gesmar, The applicability of the magnetization-transfer NMR technique to determine chemical exchange rates in extreme cases. The importence of complementary experiments, J. Magn. Reson. 49 (1982) 444–463.

[17] B.D. Nageswara Rao, Nuclear magnetic resonance line-shape analysis and determination of exchange rates, Meth. Enzymol. 176 (1989) 279–311.

[18] J.I. Kaplan, Exchange broadening in nuclear magnetic resonance, J. Chem. Phys. 28 (1958) 278–282.

[19] K.W. Penfield, A.A. Gewirth, E.I. Solomon, Electronic structure and bonding of the blue copper site in plastocyanin, J. Am. Chem. Soc. 107 (1985) 4519–4529.

[20] A.J. Vega, D. Fiat, Nuclear relaxation processes of paramagnetic complexes: the slow-motion case, Mol. Phys. 31 (1976) 347–355.

[21] M. Gueron, Nuclear relaxation in macromolecules by paramagnetic ions: a novel mechanism, J. Magn. Reson. 19 (1975) 58–66.

[22] I.A. Solomon, Relaxation processes in a system of two spins, Phys. Rev. 99 (1955) 559–565.

[23] L. Ma, M.A.S. Hass, N. Vierick, S.M. Kristensen, J. Ulstrup, J.J. Led, Backbone dynamics of reduced plastocyanin from the cyanobacterium *Anabaena variabilis*: regions involved in electron transfer have enhanced mobility, Biochemistry 42 (2003) 320–330.